Modeling the Electrophysiological Activities of Breast Tumors with Different Morphologies

Ahmed M. Hassan
Department of Electrical Engineering
University of Arkansas
Fayetteville, USA
amhassan@uark.edu

Magda El-Shenawee
Department of Electrical Engineering
University of Arkansas
Fayetteville, USA
magda@uark.edu

***Abstract*—Recently, a diffusion-drift model was developed to simulate the biopotential signals and the electric current densities generated by single and few dividing MCF-7 cells, the most studied breast cancer cell line. In this work, the modeling is extended to simulate tumors containing hundreds of dividing MCF-7 cells. The dividing cells are assembled into realistic tumor patterns generated from a multiple-nutrient tumor growth model. Primarily, three tumor patterns are investigated: papillary, comedo and compact. The numerical results show that the tumor induced biopotentials vary significantly with the tumor pattern. In addition, complex tumor patterns can result in a shift of the point of maximum biopotential away from the center of the tumor. These observations can be utilized in the future advancement of the biopotential detection of breast cancer.**

Keywords-component; Breast Cacner; Diffusion-Drift; Biopotentials; MCF-7

I. INTRODUCTION

It is well known that electrophysiological activities play a role in the regulating the growth and division of healthy and cancerous cells [1]-[2]. However, it was only recently that advances in experimental and numerical techniques have helped shed light on the mechanism by which these electrophysiological activities are generated [1]-[2]. Experimental electrophysiological measurements have shown that MCF-7 cells, the most studied breast cancer cell line, regulate their membrane potential during cell division [3]. These regulations were experimentally associated to variations in the permeability of the membranes of MCF-7 cells to potassium ions [4]. These experimental observations were simulated using a diffusion-drift model in order to understand the propagation of the biopotentials from the vicinity of the cells to a tissue boundary such as the surface of the breast [5]-[6]. The aim of the developed models was to explain the properties of the biopotentials recorded on the surface of the breast of breast cancer patients reported in [7]-[8]. The computational models developed only included single [5] or multiple cells up to 5 [6]. The logical extension of the models is to increase the number of cells to simulate the electrophysiological activity of tumors containing hundreds of dividing cells.

A key question is how to arrange this large number of cells. Tumors in the avascular growth stage exhibit a variety of different patterns which are determined by factors in the tumor microenvironment as well as interactions with healthy cells [9]. A tumor growth model developed by Ferreira *et al.* was capable of generating most of the common tumor patterns or morphologies such as papillary, comedo (tumor with central necrotic core) and compact [9].

The goal of this work is to simulate tumors with biological accurate patterns containing hundreds of cancerous cells. These biologically accurate shapes are obtained using the tumor growth model of Ferreira *et al.* reported in [9]. Consecutively, the effect of the tumor morphology on the generated biopotential signals is analyzed.

This paper is arranged as follows. Section II describes the tumor growth model and Section III describes how the tumor patterns are integrated in the diffusion-drift model. The biopotential results are shown in Section IV and the conclusions and future work are detailed in Section V.

II. MULTIPLE-NUTRIENTS TUMOR GROWTH MODEL

The reaction-diffusion tumor growth model developed by Ferreira *et al.* incorporates two nutrients. The first nutrient is essential for cell division and the second is essential for cell metabolism and survival. The presence of the two nutrients provides an additional degree of freedom which allows the generation of a larger variety of tumor patterns compared to a single nutrient model. Different tumor patterns can be generated by modeling different levels of competition for the two nutrients between healthy and cancerous cells [9]. For example, if there is a high level of competition for the nutrient necessary for cell division between cancerous and healthy cells the tumor will break into a fractal papillary pattern to increase its outer surface area to gain more access to the nutrients [9]. If there is a high level of competition for the nutrient necessary for cell metabolism between cancerous and healthy cells, cancerous cells become more likely to die and the tumor will develop a central necrotic core which is termed a comedo pattern. A compact tumor pattern is achieved by simulating moderate competition for nutrients between cancerous and healthy cells.

Three tumor patterns are generated: papillary, comedo and compact as shown in Fig. 1a, Fig. 1b and Fig. 1c, respectively, using the tumor growth model of Ferreira *et al* [9]. In order to

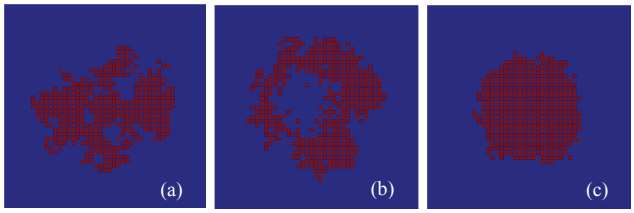

Fig. 1: (a) Papillary tumor pattern, (b) Comedo tumor pattern, and (c) Compact tumor pattern.

have a fair comparison between the biopotential signals generated by the three different patterns, the three tumors in Fig. 1 were generated to have the same number of cells, 444. In the following section, the incorporation of the tumor patterns into the diffusion-drift model is detailed.

III. Diffusion-Drift Model

The tumor patterns generated in the previous section are incorporated in the computational domain in Fig. 2 such that they all have the same center in addition to an intercellular spacing of 0.25μm as calculated in [6]. The boundary conditions of the computational domain in Fig. 2 are zero flux at the left boundary to emulate the surface of the breast, periodic boundary conditions at the top and bottom boundaries and Dirichlet boundary conditions at the right boundary using the values reported in [5]-[6].

Changes in the permeability of the membrane of dividing MCF-7 cells disturb the balance of the ions in the extracellular and intracellular media creating diffusion-drift forces that can be described using the Poisson Nernst-Plank and Continuity equations [5]-[6]:

$$\nabla^2\phi = -\frac{F}{\varepsilon}\sum_m Z_m C_m \tag{1}$$

$$\vec{J}_m = -D_m \nabla C_m - \mu_m Z_m C_m \nabla\phi \tag{2}$$

$$\frac{\partial C_m}{\partial t} = -\nabla\cdot\vec{J}_m \tag{3}$$

where ϕ is the biopotential, F is Faraday's constant (96485 C/mol), ε is the permittivity of the material ($80\varepsilon_0$ for water under quasi static conditions), Z_m is the signed valence of ion m, C_m is the concentration of ion m, $\vec{J}_m$ is the electric current density of ion m, and D_m and μ_m are the diffusion and mobility coefficients, respectively, of ion m. Potassium C_{K^+}, sodium C_{Na^+}, chloride C_{Cl^-} and negatively charged proteins C_{A^-} are incorporated in (1)-(3) due to their large impact on the membrane potential [10].Since proteins cannot penetrate the cell membrane, C_{A^-} inside the cells is fixed throughout the simulation at 135mM [5]-[6].

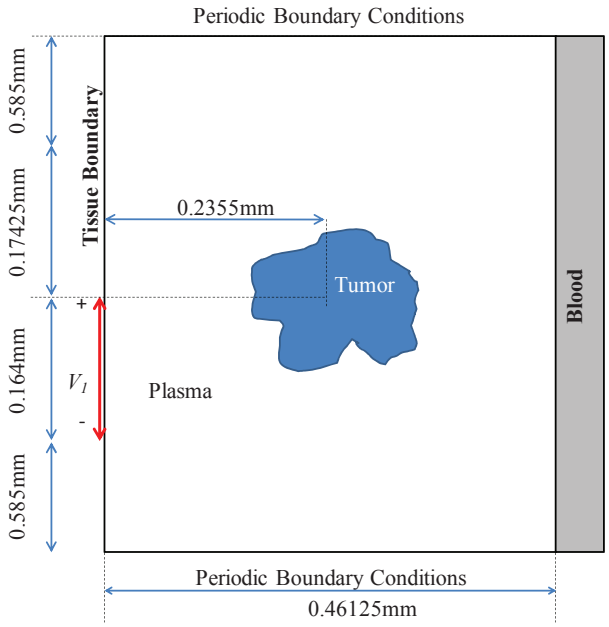

Fig. 2: The computational domain showing the tumor and the locations of the biopotential V_1.

Equations (1)-(3) are solved by discretizing them both spatially and temporally. Implicit temporal discretization is employed for numerical stability [5] and non-uniform spatial discretization is employed to accommodate the contrast in size between the size of the cell and the intercellular spacing [6]. Once discretized, (1)-(3) can be expressed as four systems of equations, one for the biopotential and one for each of the three ions C_{K^+}, C_{Na^+} and C_{Cl^-}. The majority of the computational time of the model is consumed in the solution of these systems of equations. In order to reduce the computational time the solution of these four systems of equations is parallelized using the Portable, Extensible Toolkit for Scientific Computation (PETSc) library [11]-[12]. The PETSC library contains a plethora of different solvers and pre-conditioners for solving systems of equations in parallel [13]. The Enhanced Bi-Conjugate Gradient Stabilized (*L*) iterative solver is found to be the optimum solver for the system of equations in (1)-(3). The biopotential system of equations is found to be more ill-conditioned in comparison to the ions systems of equations. Therefore, the optimum pre-conditioner for the system of equations is found to be the Additive Schwarz Method coupled with the drop tolerance Incomplete *LU* factorization [12]. The relatively simpler Block Jacobi method coupled with the zero order Incomplete *LU* factorization is found to be optimal for the ions systems of equations. Upon the utilization of these parallel solvers a maximum speedup of 15 times is achieved using 56 processors on the Star of Arkansas Supercomputer [11]-[12].

The spatial distributions of the biopotentials generated by the papillary, comedo, and compact tumor patterns are calculated. The cells in each pattern are simulated to have transitions in their membrane potentials similar to those experimentally reported in [3] and numerically simulated in

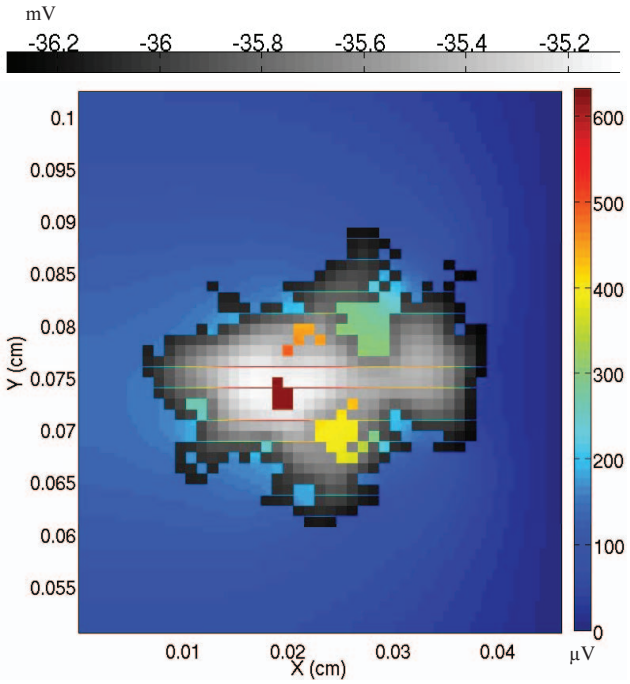

Fig. 3: The spatial distribution of the intracellular and extracellular biopotentials for the papillary pattern when all the cells are hyperpolarizing.

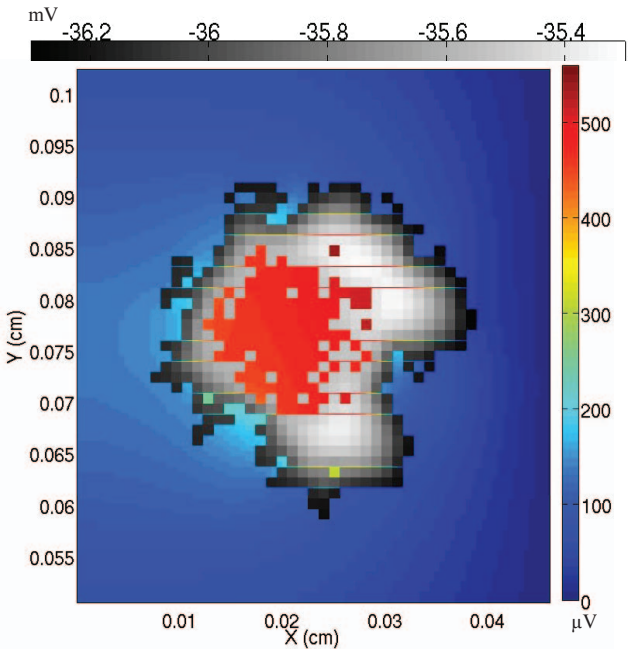

Fig. 4: The spatial distribution of the intracellular and extracellular biopotentials for the comedo pattern when all the cells are hyperpolarizing.

[5]-[6]. The membrane potential of each cell either depolarizes, becomes more positive, hyperpolarizes, become more negative or remains quiescent with no change. For each tumor pattern,

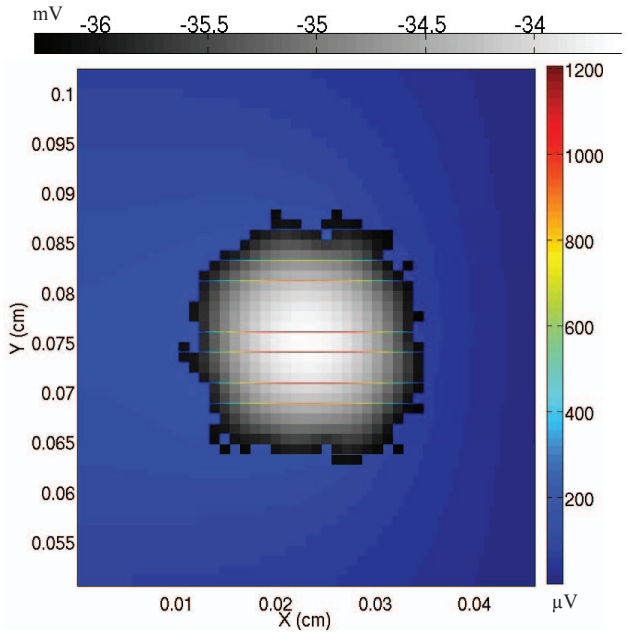

Fig. 5: The spatial distribution of the intracellular and extracellular biopotentials for the compact pattern when all the cells are hyperpolarizing.

six cases are considered: (*i*) all the cells depolarizing, (*ii*) all the cells hyperpolarizing, (*iii*) the majority of the cells depolarizing, (*iv*) the majority of the cells hyperpolarizing, (*v*) the majority of the cells quiescent, and (*vi*) equal probability of the cell depolarizing, hyperpolarizing or quiescent.

IV. Results

Fig. 3, Fig. 4, and Fig. 5 show the spatial distribution of the biopotentials when all the cells are hyperpolarizing for the papillary, comedo and compact tumor patterns, respectively. Only the case where the all the cells are hyperpolarizing is presented in Fig. 3-Fig. 5 due to space limitations. The other five cases will be presented in the conference. The figures are achieved 49 seconds from the start of the hyperpolarization transition. For clarity two color scales are utilizeed since he intracellular biopotentials are in the order of mV whereas the extracellular biopotentials are in the order of μV. The intracellular biopotential is shown in shades of gray and the extracellular biopotential is shown in color. The reference zero biopotential for the plots in Fig. 3 is the blood vessel at the right hand side of the computational domain.

In the hyperpolarization transition, the intracellular biopotential becomes more negative changing from -15mV to -42.3mV [5]-[6]. From Fig. 3-Fig. 5, it can be seen that the cancerous cells at the outer perimeter of the tumor are more negative than the cancerous cells in the interior of the tumor. Therefore, the transition is slightly faster in the cells on the outer perimeter of the tumor compared to the cells in the interior. The cells on the outer rim of the tumor have more access to the extracellular plasma and, therefore, any ions released by these cells disperse faster clearing the way for more

ions to be dispersed which explains the faster transition at the perimeter of the tumor.

In Fig. 3, the maximum extracellular biopotential is in the gaps in the tumor pattern containing no cancerous cells. This is because any ions released in those gaps have their motion restricted by the surrounding cell boundaries and, therefore, the ions accumulate causing the magnitude of the biopotentials to increase. Also, the biopotential is enhanced in the necrotic core in Fig. 4 because ions released in the necrotic core have their motion restricted by the cells in the outer perimeter of the tumor. As for the compact pattern in Fig. 5, the maximum extracellular biopotential is in the intracellular spacing and it decreases in the intercellular spacing towards the boundary of the tumor.

By comparing the maxima of the extracellular biopotentials colorbars in Fig. 3-Fig. 5, it can be seen that the pattern of the tumor has a significant impact on the generated biopotentials. Moreover, by focusing on the biopotential at the tissue boundary, x=0cm, in Fig. 3 it can be seen that the point of maximum biopotential is shifted slightly downwards in comparison to Fig. 4 even though both patterns have the same center. Therefore, it can be concluded that the complexity of the tumor pattern can lead to a shift of the point of maximum biopotential away from the center of the tumor.

V. Conclusions

The biopotential signals generated by tumors with biologically accurate patterns are modeled. Three different tumor patterns, generated using a multiple-nutrients tumor growth model, were studied. The results show that the pattern of the tumor has a large impact on the generated biopotentials. Moreover, the complexity of the tumor pattern can lead to shifts in the distribution of the extracellular biopotentials.

In the biopotential detection of breast cancer, one electrode is typically placed directly above the center of the tumor on the surface of the breast and one electrode is placed away from the tumor similar to the configuration of V_1 in Fig. 2. The results show that the point of maximum biopotential may shift in different tumor patterns, and, therefore, a possible future enhancement to the sensor arrangement would be to employ a large array of finely spaced electrodes in order to capture any shift is the biopotential away from the center of the tumor.

Acknowledgment

This work is funded in part by the National Science Foundation under award EDA-0965571 (2010 Workshop on Advances in Breast Cancer Research), Cyberinfrastructure awards EP-0918970 (CI TRAIN) and MRI-072265 (Star of Arkansas) and in part by the Doctoral Academy Fellowship at the University of Arkansas.

References

[1] J. D. Blackiston, K. McLaughlin, and M. Levin, "Bioelectric controls of cell proliferation: ion channels, membrane voltage, and the cell cycle," *Cell Cycle*, vol. 8, no. 21, pp. 3527-3536, 2009.

[2] S. Sundelacruz, M. Levin, and D. Kaplan, "Role of membrane potential in the regulation of cell proliferation and differentiation," *Stem Cell Rev.*, vol. 5, no. 3, pp. 231–246, 2009.

[3] J. Strobl, W. Wonderlin and D. Flynn, "Mitogenic Signal Transduction in Human Breast Cancer Cells," *Gen. Pharmac.*, vol. 26, no. 8, pp. 1643-1649, 1995.

[4] W. Wonderlin, K. Woodfork, and J. Strobl, "Changes in Membrane Potential During the Progression of MCF-7 Human Mammary Tumor Cells Through the Cell Cycle," *J. Of Cellular Physiology*, vol. 165, pp. 177-185, 1995.

[5] A. M. Hassan and M. El-Shenawee, "Diffusion-drift modeling of a growing breast cancerous cell," *IEEE Trans. Biomed. Eng.*, vol. 56, no. 10, pp. 2370–2379, Oct. 2009.

[6] A. M. Hassan and M. El-Shenawee, "Modeling Biopotential Signals and Current Densities of Multiple Breast Cancerous Cells," *IEEE Trans. on Biomed. Eng.*, vol. 57, no. 9, pp. 2099-2106, Sept. 2010.

[7] M. Fukuda, K. Shimizu, N. Okamoto, T. Arimura et al., "Prospective Evaluation of Skin Surface Electropotentials in Japanese Patients with Suspicious Breast Lesions," *Jpn. J. Cancer Res.*, vol. 87, no. 10, pp. 1092-1096, Oct. 1996.

[8] J. Cuzick, R. Holland, V. Barth, R. Davies, M. Faupel, I. Fentiman, H. Frischbier, J. LaMarque, M. Merson, V. Sacchini, D. Vanel and U. Veronesi, "Electropotential measurements as a new diagnostic modality for breast cancer," *The Lancet*, vol. 352, Aug., 1998.

[9] S. Ferreira Junior, M. Martins and M. Vilela, "Reaction-diffusion model for the growth of avascular tumor," *Physical Review E*, vol. 65, no. 2, pp. 021907-1-021907-8, 2002.

[10] J. Enderle, S. Blanchard and J. Bronzino, *Introduction to Biomedical Engineering*, Second Edition, Elsevier Academic Press, 2005.

[11] A. M. Hassan and M. El-Shenawee, "The MPI Parallelization of the Diffusion-Drift Algorithm for Quantitative Analysis of Breast Tumor Electric Signals," *Proc. of the IEEE Int. Symp. on Ant. and Prop. and USNC/URSI National Radio Science Meeting*, Toronto, Canada, July 11-17, 2010.

[12] A. M. Hassan and M. El-Shenawee, "Parallel Implementation of the Diffusion-Drift Algorithm for Modeling the Electrophysiological Activity of Breast Tumors," *Journal of Parallel and Distributed Computing (in review)*.

[13] S. Balay, K. Buschelman, V. Eijkhout, W. D. Gropp, D. Kaushik, M. G. Knepley, L. Curfman McInnes, B. F. Smith and H. Zhang, "PETSc Users Manual," *Technical Report ANL-95/11 - Revision 3.1*, Argonne National Laboratory, March 2010.